Ceramics International 51 (2025) 43861–43869

Contents lists available at ScienceDirect

Ceramics International

journal homepage: www.elsevier.com/locate/ceramint

Boosting the electrochemical performance of lithium-ion batteries with a $Li_3V_2(PO_4)_3$ electrode designed as a desert cactus shaped and layered with MWCNT for energy storage applications

V. Sharmila [a], J. Richards Joshua [a], M. Parthibavarman [a,*], S. Maruthamuthu [b], Adel El-marghany [c], Mtangi Mohamed Mussa [d], E. Vijayakumar [e,**], Sambasivam Sangaraju [f,***]

[a] Department of Science and Humanities, Shree Venkateshwara Hi Tech Engineering College, Erode, Tamilnadu, India
[b] PSG Institute of Technology and Applied Research, Coimbatore, Tamil Nadu, 641 062, India
[c] Department of Chemistry, College of Science, King Saud University, P.O. Box 2455, Riyadh, 11451, Saudi Arabia
[d] Department of Physics, University of Dar es Salaam, P.O. BOX 35063, Dar es Salaam, Tanzania
[e] Advanced Energy Materials R&D Division, Dongkwang Co.Ltd., Anyang-si, Gyeonggi-do, 14057, South Korea
[f] National Water and Energy Center, United Arab Emirates University, Al Ain, 15551, United Arab Emirates

ARTICLE INFO

Handling editor: Dr P. Vincenzini

Keywords:
$Li_3V_2(PO_4)_3$
Insitu pattern
Monoclinic
NASICON
MWCNT

ABSTRACT

$Li_3V_2(PO_4)_3$ (LVP) stands out as a promising cathode material due to its higher operating voltage and theoretical capacity, effectively addressing continuous demands. At elevated operating voltages, the electrochemical performance of pure LVP is significantly constrained. This study involved the synthesis of multiwalled carbon nanotubes (MWCNTS) -decorated LVP using a hydrothermal-assisted solid-state method. Employing a range of techniques, the crystalline phase, morphology, microstructure, and composition of the resulting materials were examined. The findings from transmission electron microscopy reveal that the crystalline LVP surface is enveloped by an amorphous carbon layer roughly 3–5 nm thick, with the LVP particles linked by carbon. The evaluation of the electrochemical performance of the LVP cathode at a cut-off voltage of 4.2 V was conducted. The performance of the prepared electrodes was evaluated through electrochemical analysis, which indicated that $Li_3V_2(PO_4)_3$ coated with multi-walled carbon nanotubes (MWCNTs) exhibited a capacity of 183 mAh g^{-1} at 100 A g^{-1}. Additionally, in situ XRD patterns were obtained throughout the charging and discharging cycles, indicating that the MWCNT coating contributed to the formation of extra active sites and improved electrode stability over extended cycling periods. Nanostructured $Li_3V_2(PO_4)_3$ hybrid cathodes enhance electrical conductivity, offer extensive electrode/electrolyte contact surfaces, facilitate the movement of electrons and Li^+, and adeptly manage strain during the insertion and extraction of Li^+. The recent advancements in the application of 0D (nanoparticles), 1D (nanowires and nanobelts), 2D (nanoplates and nanosheets), and 3D (nanospheres) $Li_3V_2(PO_4)_3$ for high-performance lithium-ion batteries emphasise their fabrication methods and distinctive electrochemical characteristics. The results demonstrate that MWCNT-coated $Li_3V_2(PO_4)_3$ could function as a cost-efficient, highly stable, and high-performance electrode for Lithium-ion energy storage applications.

1. Introduction

Probably the most momentous and consequential inventions of the twentieth century were the introduction of lithium rechargeable batteries. These batteries are particularly high-energy density and high-capacity. The advent of Li-ion batteries has been a game-changer for the many multipurpose, portable devices that we use every day. Much study has focused on lithium rechargeable batteries because of their possible

* Corresponding author.
** Corresponding author.
*** Corresponding author.
E-mail addresses: varmanphysics85@gmail.com (M. Parthibavarman), evijayakumarindia@gmail.com (E. Vijayakumar), s_sambasivam@uaeu.ac.ae (S. Sangaraju).

https://doi.org/10.1016/j.ceramint.2025.07.117
Received 1 May 2025; Received in revised form 2 July 2025; Accepted 9 July 2025
Available online 10 July 2025

applications in energy storage systems and electric cars [1]. In recent years, phosphate-containing polyanion composite materials such as $LiVPO_4F$, $LiMnPO_4$, and $Li_3V_2(PO_4)_3$ (LVP) have attracted significant scientific interest [1]. The LiVPO4F material demonstrates a high operating voltage of 4.2 V, making it interesting for high-voltage batteries; nevertheless, it suffers from poor cycle performance. $LiMnPO_4$ exhibits a high, stable voltage [2], although its electrochemical activity is largely ineffective for lithium-ion extraction [3]. Monoclinic LVP, a potential substitute for commercial layered cathodes, is characterised by its low cost and high discharge capacity, achieving 198 mAh g^{-1} when charged to 4.8 V, rendering it an optimal material for many cathode applications. Nevertheless, the charging voltage is excessively high, leading to electrolyte breakdown; thus, the sample is often tested at voltages ranging from 3.0 to 4.3 V, achieving a corresponding capacity of 133 mAh g^{-1}.

Because of its open three-dimensional (3D) structure, LVP shows a higher rate of lithium-ion migration than $LiFePO_4$, but its low electronic conductivity makes it unsuitable for use in large-scale power devices in electric vehicles. Fortunately, various techniques exist to enhance the specific capacity and cycling performance of LVP cathode material at elevated rates. According to Bhuvaneswari et al. [4], the most effective method is to apply a thin layer of carbon to the surface of LVP particles. This is the most helpful method. According to the findings of their experiment, the thickness of the coating and the amount of carbon present both play a significant effect in determining the electrochemical characteristics and the electronic conductivity of the material. Furthermore, different carbon sources have varying effects on the physicochemical and electrochemical properties [5], which is why it is essential to do additional study about the appropriate carbon source. Recently, carbon nanotubes (CNT) have been considered as a novel carbon source due to their exceptional electronic and mechanical properties [6]. These properties can be attributed to the high specific surface area and good conductivity around (1–4) × 102 S cm^{-1} along the CNT axis and 5–25 S cm^{-1} perpendicular to the axis, respectively [7]. At the same time, based on CNT's capillarity and surface tension, the electrolyte can be absorbed and thus reduce the polarization of the interface. And the CNT also provides a direct path for lithium-ion transport to improve its electrochemical properties [8]. As a result of the ability to produce a more integrated conductive network between the active materials and the substrate, it has been suggested that MWCNTs are ideal enhancements to utilise in the electrode. The total capacity of the batteries that had CNT additives in the electrodes was larger, and the high-rate discharge performance of these batteries was improved [9,10]. Recently, MWCNTs have been utilized as a conductive carbon addition in the process of creating composites consisting of $LiFePO_4$/MWCNTs [11,12] and $LiCoO_2$/MWCNTs [13]. MWCNTs were used as the conducting additive in $LiFePO_4$ by Li et al. [11], and they discovered that the inclusion of MWCNTs was an efficient technique to boost rate capability and cycle efficiency. According to Jin et al. [12], the incorporation of MWCNTs into $LiFePO_4$ not only results in an increase in the electronic conductivity and the lithium-ion diffusion coefficient, but it also results in a reduction in crystallite size and charge-transfer resistance characteristics [14–21]. Moreover, LVP serves as a material suitable for both cathode and anode applications, enabling the fabrication of a symmetric cell. The symmetric cell offers the benefit of eliminating the process of utilising various active materials, hence decreasing costs. Motivated by these factors, we will propose a pragmatic approach for carbon coated electrodes via the innovative design of the LVP.

This study discusses the synthesis of an LVP@MWCNTs composite utilising multiwalled carbon nanotubes (MWCNTs) through the hydrothermal-assisted solid-state method. The MWCNTs can efficiently interconnect the isolated fine LVP particles, significantly improving the electrochemical performance of the LVP@MWCNTs composite, particularly at elevated current densities, such as providing a steady capacity of 183 mAh g^{-1} at 100 A g^{-1}.

2. Experimental procedure

2.1. Fabrication of $Li_3V_2(PO_4)_3$ @MWCNT composite

2.1.1. The fabrication process of the $Li_3V_2(PO_4)_3$@MWCNT

All the chemicals were used without any further purification. Multiwall carbon nanotubes (>90 % MWCNT, basis, with a diameter of 20–30 nm and a length of 0–8 μm) were purchased from Bayar company, India. In 30 ml of deionised water and 20 ml of ethylene glycol (EG), we mixed stoichiometric amounts of $C_2H_3LiO_2$, V_2O_5, and $NH_3.H_2PO_4$. We agitated the solution for 30 min to ensure a thorough amalgamation. We moved the finished mixture into a stainless-steel autoclave that was lined with Teflon and had a volume of 100 ml. The autoclave underwent a temperature of 180 °C for a duration of 10 h. The hydrothermal reaction enabled the transformation of the solution into a suspension. To get rid of any leftover chemicals or contaminants, the product was cleaned using a solution of deionised water and 100 % ethanol once the hydrothermal reaction was finished. We annealed the purified product at a temperature of 650 °C for 6 h, designating the resultant sample as LVP. The solid-state method was used to make the $Li_3V_2(PO_4)$ @MWCNT composite. It was ground with a mortar and pestle in 1:1 and 1:3 (LVP: MWCNT) ratios.

The cathode material's packing quantity was carefully controlled because it has a big impact on the electrochemical performance. It was observed that a material mass lower than 2.5 g led to ion disintegration during cycling in the electrolyte. Precise quantities of $Li_3V_2(PO_4)_3$@MWCNT were measured for the composite fabrication. For the coated samples, LVP@MWCNT was utilized. The prepared samples, namely LVP and LVP@MWCNT, were obtained and ready for further characterization. For a better understanding of the fabrication process, refer to Fig. 1, A simplified representation of the steps used to create LVP coated with MWCNTs.

2.2. Characterization techniques

This X-ray diffraction (XRD) technique, coupled with CuKα radiation (λ = 1.5406 nm), was used by Bruker to examine the materials' structural characteristics. The structure of the particles and chemical content were examined using a scanning electron microscope (JEOL Model JSM - 6390 LV). XPS tests were conducted at an electron take-off angle of 45° with an energy of 11.7 eV to acquire the photoelectron spectra.

2.3. Electrode preparation

The elements used to make the combined electrodes were mixed at a ratio of 8:1:1. The AC or LVP@MWCNT active material, Super P carbon conductive carbon, and acetylene black-2 adhesive are all part of this. The composition was meticulously blended to guarantee uniformity. An aluminium plate served as the current collector after compressing the electrode combination that had resulted. The aluminium plate possessed an area of 200 mm^2 and a thickness of 0.25 mm. The electrode that was used was allowed to dry in a vacuum at 60 °C overnight. For single-electrode research, a half-cell configuration was established by utilising the prepared electrode as both the counter and reference electrode. The assembly occurred within an Argon-filled glove box to preserve an inert atmosphere. A 1M LiPF6 solution was used for the electrolyte. Ethylene carbonate and diethyl carbonate were combined in an electrolyte at a volume ratio of one to one. Cyclic voltammetric studies were conducted using slow scans of 0.1 mVs^{-1}, and the data were recorded using a Solartron 1470 F instrument. At room temperature, researchers used a Neware BTS system to conduct discharge-charge galvanostatic experiments.

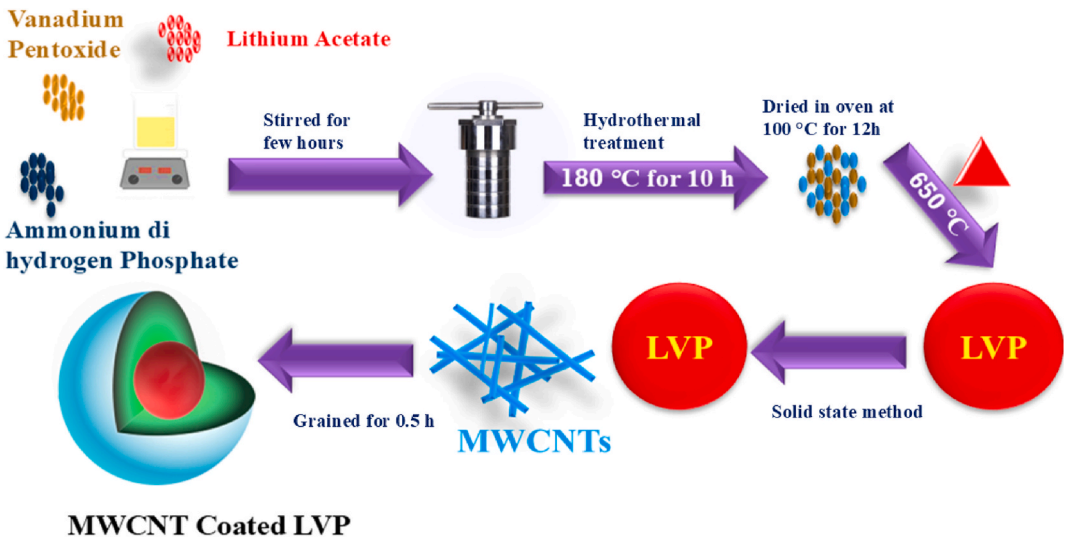

Fig. 1. A simplified representation of the steps used to create LVP coated with MWCNTs.

3. Result and discussion

3.1. XRD analysis

The LVP@MWCNT composite was synthesized by a rapid hydrothermal technique, and it possesses an improved redox potential [22–24]. The use of a carbon coating improved the material's ability to conduct electricity. This method facilitates the creation of pathways for electron migration to the current collector, thus increasing the overall conductivity [25,26]. Fig. 2a displays the recorded XRD pattern along with the results of the refining (Fig. 2b-d). In the P21/n space group, the LVP@MWCNT composite displayed a refined monoclinic phase. The values of the refined lattice parameters were found to be (a) 8.52 Å, (b) 8.59 Å, (c) 12.11 Å, and $\beta = 90.00^0$, which agrees with the values described in the literature. The LVP material exists in monoclinic and rhombohedral phases, resembling NASICON materials' structures. An effective transit of lithium ions into and out of the system is made possible by the existence of the monoclinic structure [27]. This structure consists of octahedral units comprising VO_6 and PO_4 groups, slightly distorted and connected via oxygen atoms. Lithium ions are situated at three different crystallographic sites inside the three-dimensional structure: Li (1) is in the tetrahedral spot, while Li (2) and Li (3) are in similar but different places [23]. The simulated structure of LVP was shown in Fig. 2e. The high mobility of Li ions within the LVP@MWCNT composite indicates the material's ability to accommodate high current loads, demonstrating its potential for high-performance applications

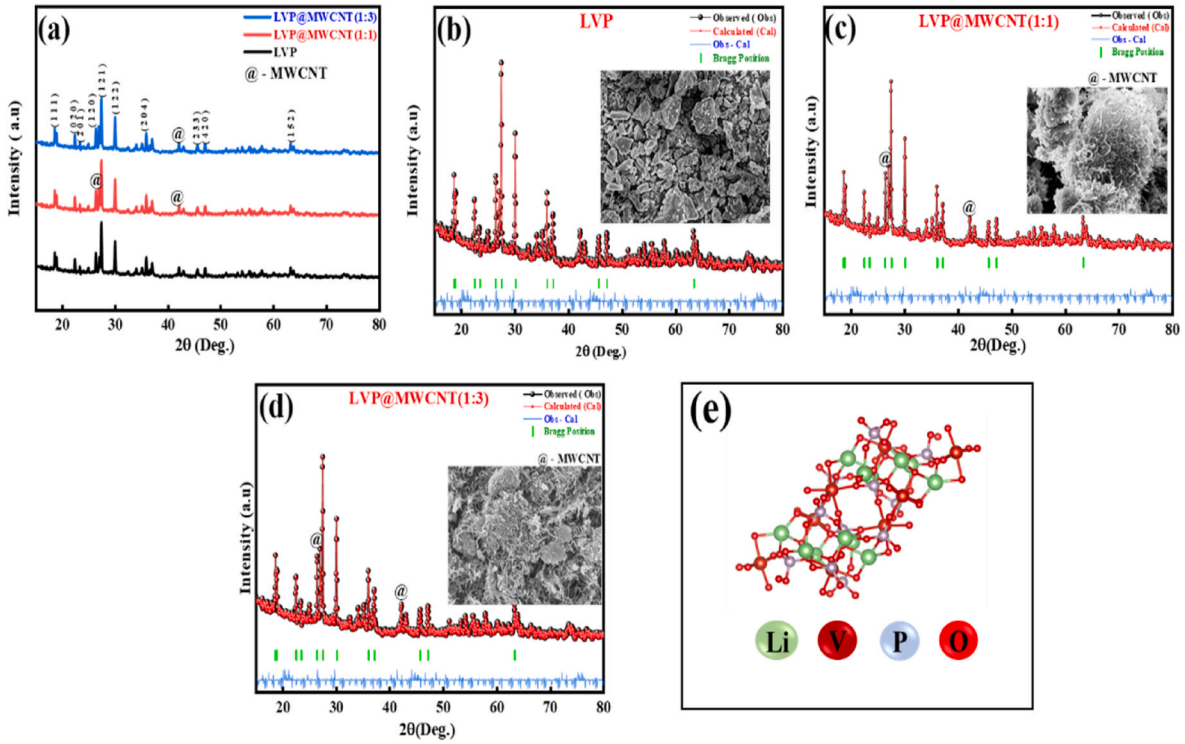

Fig. 2. (a) Diffraction pattern of the pure LVP and carbon coated LVP samples; Rietveld refinement of (b) pristine LVP (c) LVP@MWCNT (1:3); (d)LVP@MWCNT (1:3); (e) refined structure of LVP.

[28,29]. The refinement values are shown in Table 1.

3.2. FE – SEM and HRTEM analysis

Fig. 3 showcases the surface morphology and nanoscale microstructure of both pristine and MWCNT-coated LVP powders, as observed through scanning electron microscopy. The modification with MWCNT does not significantly alter the size and distribution of the LVP material. Both the pure LVP and MWCNT-coated LVP samples (LVP@MWCNT) exhibit a uniform particle distribution, with an average particle size of approximately 200 nm. The pristine LVP particles display a desert cactus-like structure (Fig. 3a). This unique morphology can facilitate efficient electron transport and contribute to improved rate capacities. Fig. 3b and c presents FESEM images of MWCNT-coated LVP at different ratios (1:1 and 1:3). These images confirm the successful coating of MWCNT on the surface of LVP, forming a wrapping-like structure. Notably, a fine cloud-like formation is observed at the tip of the cactus, which can be attributed to the presence of MWCNT on the LVP surface. The findings of Ref. [30] indicate that the synthesized LVP@MWCNTs (1:3) composite material is appropriate for conventional electrode fabrication methods. According to various papers [31,32], shape and particle size significantly influence the electrochemical performance of LVP; hence, LVP@MWCNTs(1:3) exhibits superior performance.

Additional confirmation of the MWCNT coating on the LVP surface is provided by HRTEM pictures (Fig. 3d). The estimated thickness of the MWCNT covering is 2.82 nm (as shown in Fig. 3e and f). In addition to preventing particle aggregation, the presence of rich pores and carbon covering work together to hinder Li extraction from different places during electrochemical reactions. These factors contribute to improved electrochemical performance and stability in LVP@MWCNT electrodes. The elemental mapping confirms that uniform distribution of LVP (Li, V, P, O) in the composite and also confirms the present of carbon on the prepared composites. The elemental mapping and edax spectrum were shown in Fig. 4.

3.3. XPS and BET analysis

LVP and LVP@MWCNT were subjected to X-ray photoelectron spectroscopy (XPS) analysis to learn more about their surface chemistry. In agreement with the findings from X-ray diffraction (XRD) analysis, the XPS examination demonstrated the existence of Li, P, V, O, and C elements (Fig. 5a). The whole XPS spectrum of LVP@MWCNT clearly showed the Li 1s peak at approximately 60 eV, indicating the accurate detection of lithium peaks by the precise equipment used [33]. Fig. 5a presents the high-resolution XPS spectra for the elements Li, P, O, and V. The XPS spectrum for phosphorus (P2p) displayed peaks at 135.33 eV ($P2p_{3/2}$) and 145.22 eV ($P2p_{1/2}$), indicating the presence of the $(PO_4)_3$ phosphate group (Fig. 5b). The high-resolution XPS spectra for $V2p_{3/2}$ and $V2p_{1/2}$ exhibited binding energies at 643 eV and 655 eV, respectively, indicative of V^{3+} oxidation state (Fig. 5c). Notably, there were no discernible peaks within the energy range of 648–650 eV, suggesting the absence of V^{4+} or V^{5+} species [34]. The spectrum of Li is shown in Fig. 5d. The XPS spectrum for carbon (C) revealed characteristic peaks for C=O and C-OH at binding energies of 482.6 eV and 486.3 eV, respectively (Fig. 5e) [35]. The peak at 530.56 confirms the presence of O1s as demonstrated in Fig. 5f.

Nitrogen adsorption and release tests were conducted to evaluate the porosity, which is important for storing lithium. As shown in Fig. 6, the taken samples of LVP and LVP@MWCNT performed well at 77 K. According to the data, the synthetic LVP@MWCNT (1:3) material has a significantly higher surface area and pore volume than both LVP and LVP@MWCNT (1:1), with the former having a total surface area of 30.4861 m^2 g^{-1} and the latter having a pore volume of 0.286412 cm^3 g^{-1}. The elevated overall surface area and pore volume values for the LVP@MWCNT (1:3) result from the carbon coating on the surface of the LVP.

3.4. Electrochemical performance

The CV measurements were carried out in order to investigate the electrochemical characteristics of the LVP and LVP@MWCNTs electrodes in their as-synthesized form. Fig. 6a shows the CV curves of electrodes at different scan rates of 0.5 mV s^{-1} from 2.0 to 4.2 V. This was done to look into how the scan rate affected the redox responses of the electrodes. Three cathodic peaks appeared at 3.5, 3.6, and 4.0 V, while three anodic peaks appeared at 3.6, 3.7, and 4.1 V, as seen in Fig. 7a. The good reversibility of the lithium-ion extraction/insertion processes in the LVP@MWCNT(1:3) composite is indicated by the modest voltage difference of around 0.1 V between the anodic and cathodic peaks. The electrochemical reactions are written as [36–38].

$$Li_{3.0}V_2(PO_4)_3 - 0.5Li^+ - 0.5e^- \quad Li_{2.5}V_2(PO_4)_3 \tag{1}$$

$$Li_{2.5}V_2(PO_4)_3 - 0.5Li^+ - 0.5e^- \quad Li_{2.0}V_2(PO_4)_3 \tag{2}$$

$$Li_{2.0}V_2(PO_4)_3 - 1.0Li^+ - 1.0e^- \quad Li_{1.0}V_2(PO_4)_3 \tag{3}$$

Two plateaus correspond to the reactions that are described in equations (1) and (2). According to equation (3), the third plateau, which occurs at 4.10 V, can be attributed to an additional lithium extraction from $Li_{2.0}V_2(PO_4)_3$. During the ensuing discharge phase, these reactions are extremely reversible once they have occurred. Fig. 7b-d illustrates the initial GCD curves of LVP@MWCNTs composite materials at ratios of 1:1 and 1:3, measured at a rate of 100 A g^{-1} throughout the voltage range of 2.0–4.2 V. The charge curves exhibit three plateaus at 3.59, 3.67, and 4.08 V, indicative of a series of phase changes. Discharge curves exhibit three plateaus at 3.58, 3.67, and 4.05 V, indicating two phases associated with the reduction process. With MWCNTs doping in the ratios of 1:1 and 1:3, respectively, LVP@MWCNTs composites had an initial discharge capacity of 183 and 164 mAh g^{-1}, as shown in Fig. 7b–d. The LVP@MWCNTs (1:3) sample has the highest initial discharge capacity. It is possible that MWCNTs involves in the formation of pure monoclinic LVP-coated carbon particles with smaller particles. These particles have a relative greater specific surface area, which makes it much easier for lithium to diffuse through them and results in improved electrochemical performances. The carbon covering significantly lessens the likelihood of side reactions and the breakdown of Li ions. The charge/discharge curves of the carbon-coated samples exhibit a smoother behavior, indicating improved electrochemical performance. The rate of discharge verifies that the electrode efficiency was significantly improved by covering them with carbon. Notably, the voltage profiles for Li extraction exhibit two distinct smooth voltage plateaus, while the corresponding insertion process displays a single voltage plateau [39,40].

The rate capability is a key electrochemical feature of a lithium-ion battery essential for high-power applications. For the LVP samples, the capacity values are approximately 158,149,139,128,116,102, and 92

Table 1
The Rietveld refinement results.

Sample	Crystal System	Space Group	a (Å)	c (Å)	R_P	WR_P	Gof
LVP	Monoclinic	P21/n	8.52	12.11	2.68	4.45	1.86
LVP@MWCNT(1:1)	Monoclinic	P21/n	8.63	12.21	2.36	4.19	1.33
LVP@MWCNT(1:3)	Monoclinic	P21/n	8.77	12.38	2.12	4.01	1.09

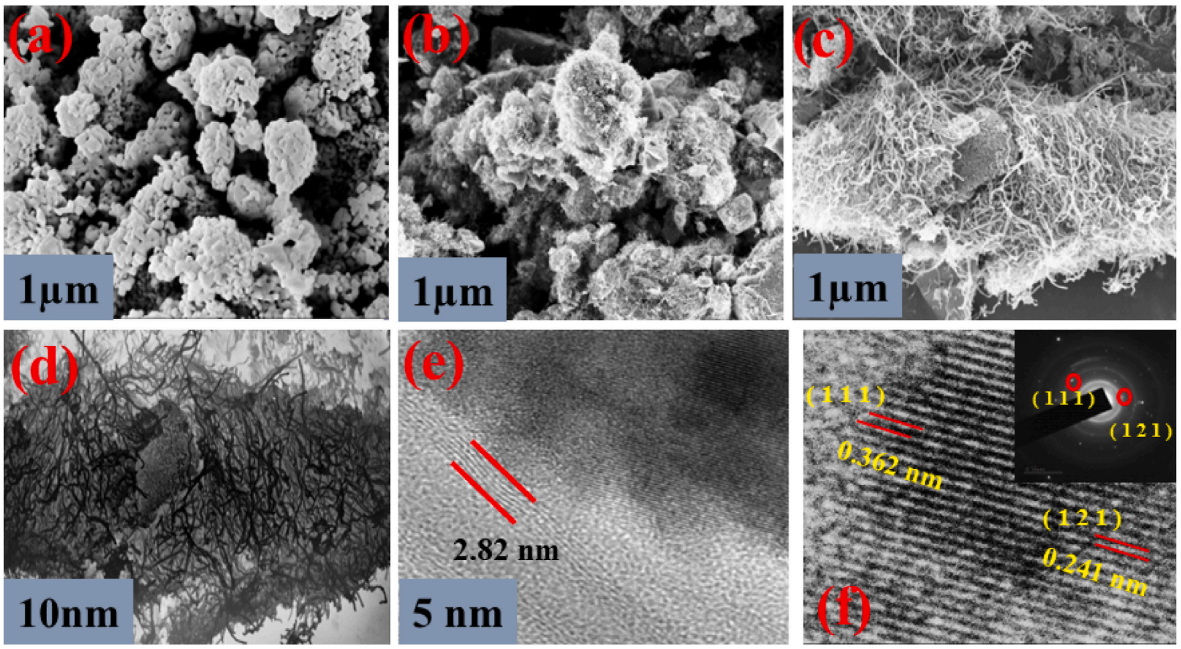

Fig. 3. FESEM images (a) LVP (b) LVP@ MWCNT (1:1); (c) LVP@MWCNT (1:3) (d–f) HRTEM images of LVP@ MWCNT (1:3).

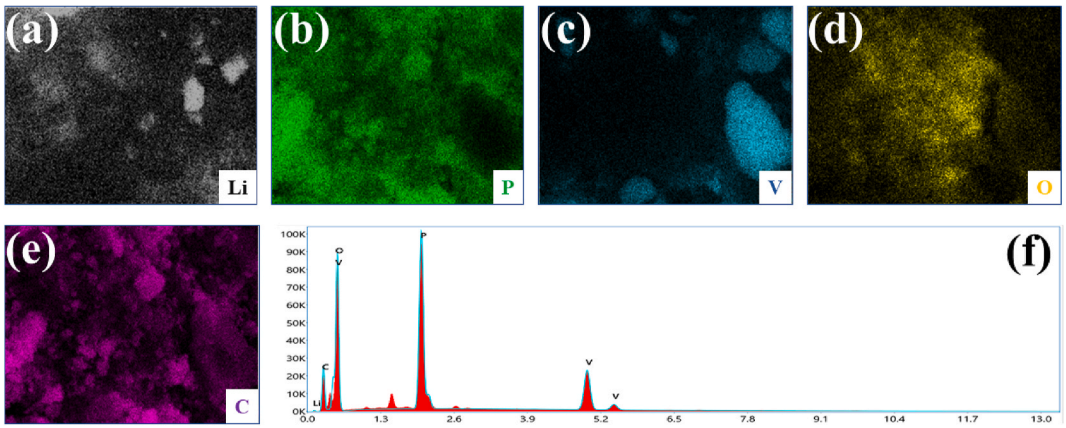

Fig. 4. Elemental mapping (a) Li; (b) P; (c) V; (d) O; (e) C; (f) EDAX spectrum of prepared sample.

mAh g^{-1} at 100–2000 Ag^{-1}, respectively. LVP@MWCNT (1:1) exhibits capacities of about 163, 156, 144, 136, 128, 112, 104, and 136 mAh g^{-1} at the same current densities. LVP@MWCNT (1:3) demonstrates superior rate performance, delivering capacities of approximately 183, 172, 163, 152, 141, 129, and 116 mAh g^{-1} at 100–2000 Ag^{-1}. This indicates that LVP@CNT (1:3) exhibits the highest rate of performance among the studied compositions compared to LVP and LVP@MWCNT (1:1) (Fig. 7e). The incorporation of multi-walled carbon nanotubes in the $Li_3V_2(PO_4)_3$ structure results in reduced capacity loss and smaller polarization during cycling. For 5000 cycles, the cathode that was doped with multi-walled carbon nanotubes retained 95 % of its initial capacity, while the pure cathode retained 90 % (Fig. 7f) [42–47]. Fig. 8 (a, b) presents the in situ XRD patterns of the prepared samples during charge and discharge profiles. The patterns produced by XRD show that the first $Li_3V_2(PO_4)_3$ phase has a NASICON structure, but when the samples are charged, a new phase similar to NASICON forms during lithium extraction, showing that the volume of the MWCNT-coated LVP samples has decreased. The Bragg peaks of LVP@MWCNT (1:1) and LVP@MWCNT (1:3) are closely aligned, indicating similar lattice parameters. The in-situ analysis confirms the stability and reversibility of the samples during the charge and discharge processes. The observed peak shifting in the XRD patterns of LVP indicates the absence of active sites during lithium extraction, resulting in a loss of electrons at high current density rates. In contrast, the peak shifting is minimal for the MWCNT-coated samples, indicating improved stability. These findings align with the FESEM images of the samples before and after cycling (Fig. 8c), supporting the notion that MWCNT-coated samples create more active sites, enabling efficient electron transport and enhanced Li extraction from various sites.

Fig. 8d and e illustrate the Nyquist plots of LVP and LVP@MWCNT (1:1, 1:3) recorded at a charge potential of 3.6 V, both prior to and following cycling. To elucidate the AC impedance spectrum of the electrodes, an equivalent circuit has been constructed in Fig. 5a. Rs denotes the solution resistance of the electrolyte; Rl and CPEl signify the migration resistance of lithium ions and the capacity of the surface layer, respectively; R2 and CPE2 represent the charge-transfer resistance and double-layer capacitance, respectively; W indicates the diffusion-controlled Warburg impedance [41–43]. The R1 values for the two electrodes are comparable, with LVP@MWCNT(1:3) measuring 4.62 Ω and LVP measuring 4.83 Ω, both significantly lower than the R1 and R2 values. The lithium-ion migration resistance Rl of LVP@MWCNT(1:3) and LVP is 12.68 and 20.38, respectively. The simulated charge-transfer

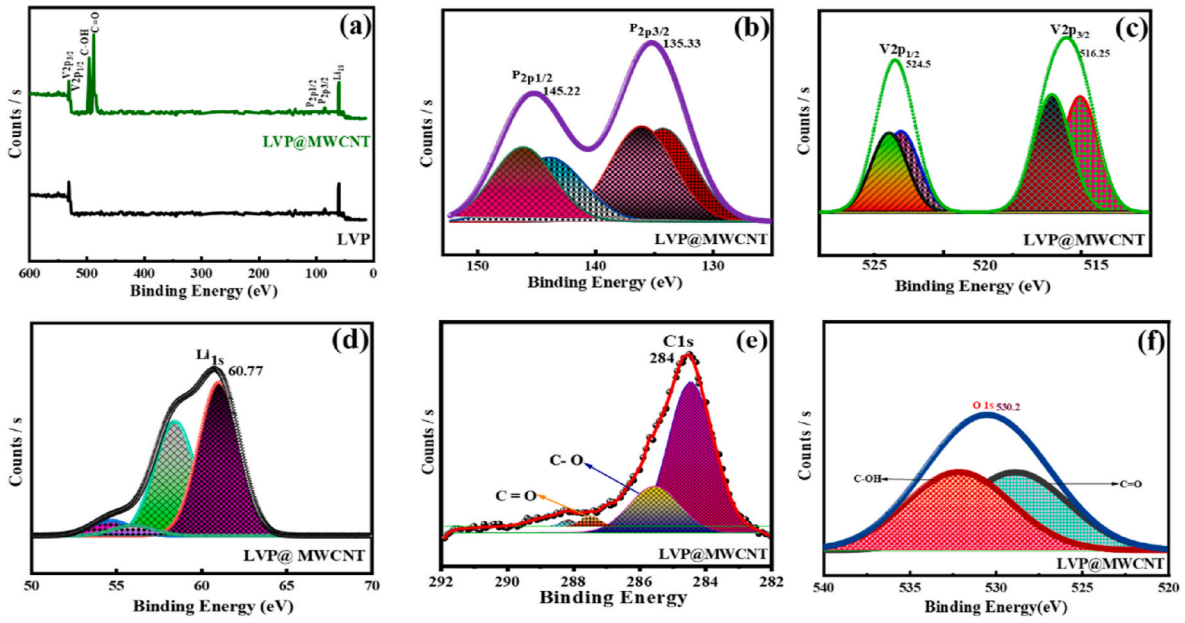

Fig. 5. XPS of LVP and LVP@MWCNT (1:3) (a) survey; (b) P 2p; (c) V 2p; (d) Li 1s; (e) C 1s; and (f) O 1s.

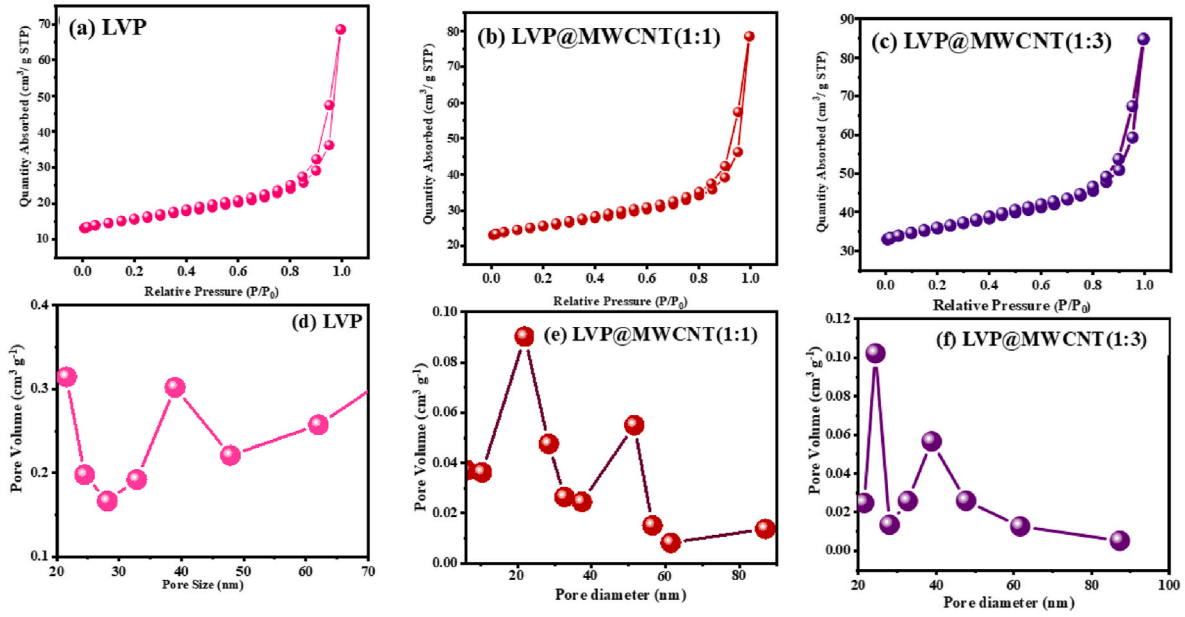

Fig. 6. The nitrogen isotherms of (a) LVP; (b) LVP@ MWCNT (1:1); (c) LVP@ MWCNT (1:3); pore distribution (d) LVP; (e) LVP@ MWCNT (1:1); (f) LVP@ MWCNT (1:3).

resistance R2 for LVP@MWCNT(1:3) and LVP is 26.32 Ω and 48.66 Ω, respectively. The LVP@MWCNT(1:3) and LVP electrodes have reduced charge transfer resistance, indicating that the conductive network formed by MWCNTs significantly enhances the conductivity of active materials and markedly decreases impedance. The diffusion coefficient of Li + can be derived from the following Eq. (1) [45,46] or Eq. (2) [47].

$$DLi = \frac{1}{2}\left(\frac{v_m}{FA\sigma_w}\right)^2 \left(\frac{\mathrm{d}\epsilon}{\mathrm{d}x}\right)^2 \quad (1)$$

$$DLi = \frac{R^2T^2}{2A^2n^4F^4\sigma_w^2C^2} \quad (2)$$

Vm represents the molar volume, F denotes the Faraday constant, A signifies the active surface area, w indicates the Warburg factor, dE/dx refers to the gradient of the open-circuit voltage relative to mobile Li + concentration, DLi is the apparent diffusion coefficient, R is the gas constant, T is the absolute temperature, n corresponds to the number of electrons per molecule during oxidation, and C is the molar concentration of Li+. At a charge state of 3.6 V, the electrochemical reaction occurs within the two-phase area. The value of dE/dx is nearly zero [45, 46], rendering Eq. (1) insignificant. Consequently, we utilise Equation (2) to compute the apparent DLi values.

The σω was ascertained as the slope of Zre vs $\omega^{-1/2}$ in the Warburg region [25,32]. Accordingly, from Equation (2), the apparent diffusion coefficients of Li-ions for LVP@MWCNT(1:3) and LVP are 5.6×10^{-9} and $2.1 \times 10{-}9$, respectively. The diffusion coefficient of LVP@MWCNT (1:3) is augmented by the incorporation of MWCNTs, attributable to their superior electronic conductivity. Fig. 8e shows the Nyquist plot of

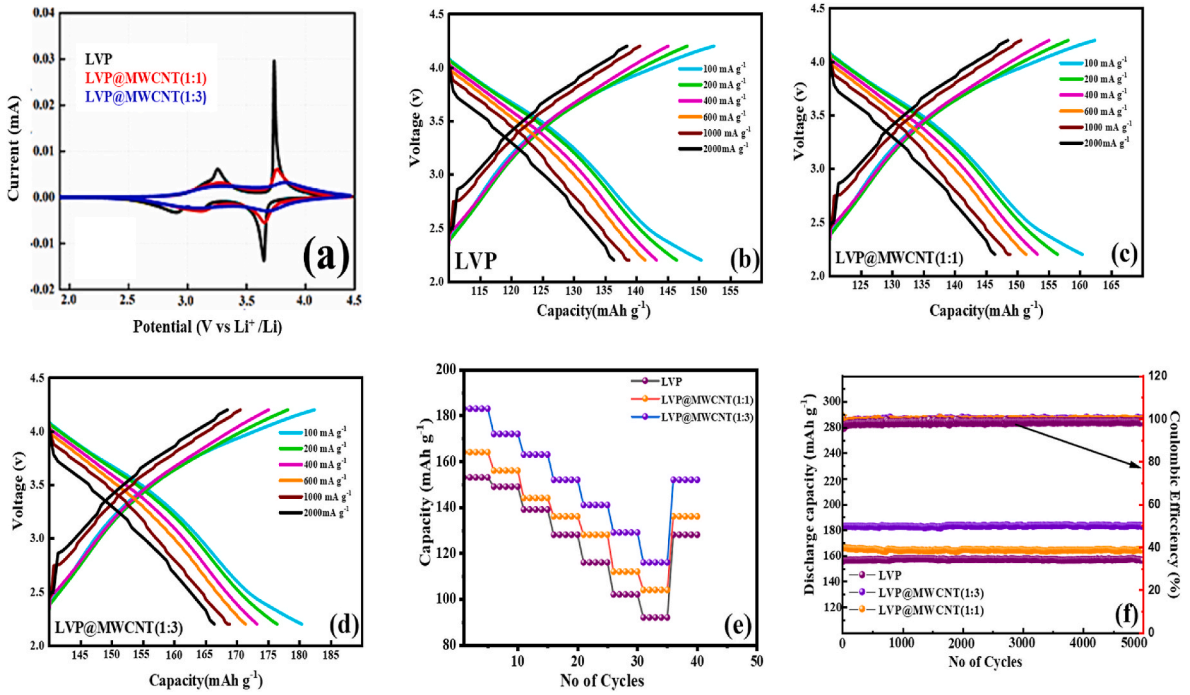

Fig. 7. (a–c) Cyclic Voltametry of LVP, LVP@ MWCNT (1:1) and LVP@MWCNT (1:3); Charge/discharge patterns of (d) LVP; (e) LVP@MWCNT (1:1); (f) LVP@MWCNT (1:3); (g) Rate performance; and (h) Stability performance of LVP and CNT coated LVP sample.

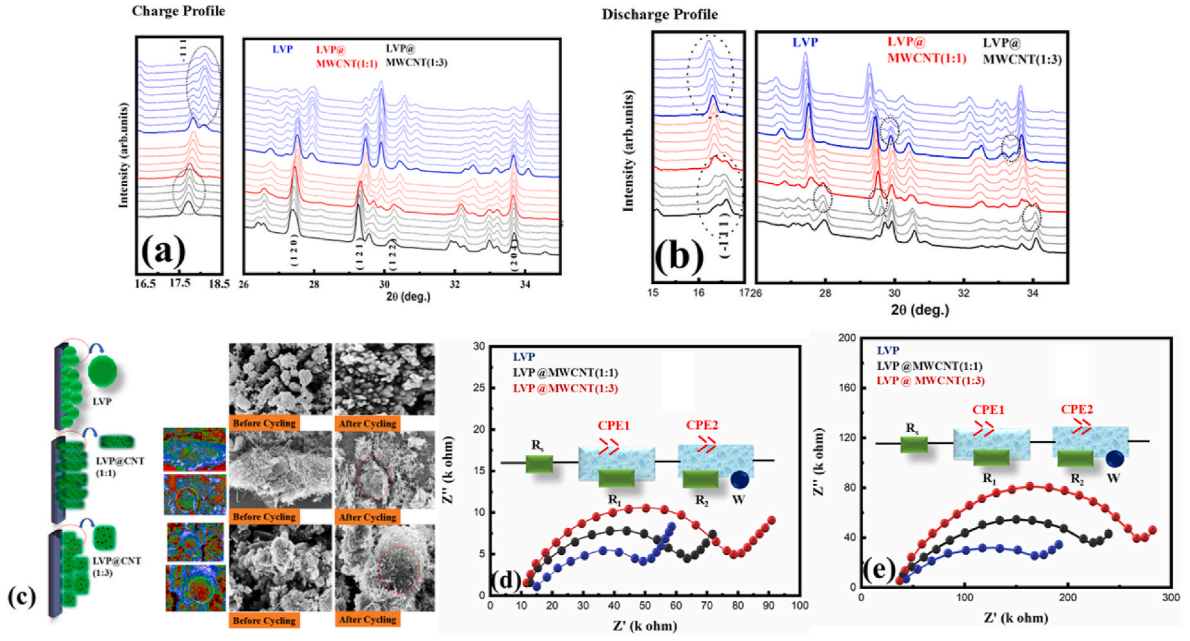

Fig. 8. Insitu XRD pattern (a) Charge profile (b) discharge profile (c) FESEM images before and after Cycling Nyquist plots of (d) before cycling; (e) after cycling.

the samples recorded after cycling, confirming that MWCNT-coated $Li_3V_2(PO_4)_3$ delivers the highest electrochemical performance with good stability and high-capacity retention. A comparison table with previous works [48–53] is presented in Fig. 9, highlighting the improved performance of MWCNT-coated $Li_3V_2(PO_4)_3$ with capacity retention.

4. Conclusion

In summary, this investigation introduces $Li_3V_2(PO_4)_3$@MWCNT as a prospective electrode material for lithium hybrid batteries, which was synthesized through a hydrothermal-assisted solid-state method. According to XRD and SEM studies, the composite electrode that was produced has a structure similar to NASICON, and it has a distinct brain-like shape due to the uniform decoration of LVP on the MWCNTs. We learnt more about the valence states and chemical makeup of the samples from the XPS results. Testing was conducted on the $Li_3V_2(PO_4)_3$@MWCNT electrochemical performance throughout a voltage range of 2–4.5 V. A specific capacity of about 183 mAh g^{-1} is produced by the carbon coating on the surface of the $Li_3V_2(PO_4)_3$ electrode, which greatly improves its electrochemical performance. Furthermore, the electrode demonstrates excellent capacity retention, with around 90 % retention after 5000 cycles. These findings highlight the enhanced

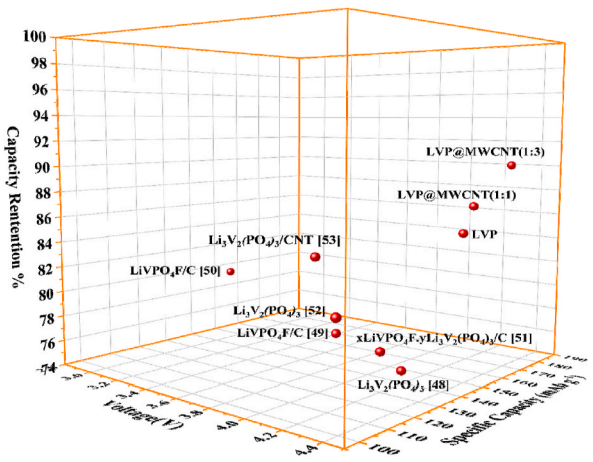

Fig. 9. Comparison with the previous work.

electrochemical performance and stability achieved through the incorporation of carbon nanotubes. The results suggest that MWCNT-coated $Li_3V_2(PO_4)_3$ represents a promising electrode material for hybrid energy storage devices. The advanced electrochemical performance, high-capacity retention, and stability make it a viable candidate for applications in energy storage systems. Improved and enhanced $Li_3V_2(PO_4)_3$@MWCNT electrodes can add to the arsenal of dependable and effective hybrid battery storage devices.

CRediT authorship contribution statement

V. Sharmila: Writing – original draft, Methodology, Conceptualization. **J. Richards Joshua:** Writing – original draft, Investigation, Conceptualization. **M. Parthibavarman:** Supervision, Formal analysis, Data curation. **S. Maruthamuthu:** Validation, Data curation. **Adel Elmarghany:** Funding acquisition, Conceptualization, Writing – review & editing. **Mtangi Mohamed Mussa:** Visualization, Formal analysis. **E. Vijayakumar:** Writing – review & editing, Formal analysis, Conceptualization. **Sambasivam Sangaraju:** Writing – review & editing, Investigation, Funding acquisition, Conceptualization.

Data availability statement

The data that support the findings of this study available from the corresponding author upon reasonable request.

Declaration of competing interest

The authors declare that they have no known competing financial interests or personal relationships that could have appeared to influence the work reported in this paper.

Acknowledgment

UAEU-AUA joint research program under grant number 12R248, and National Water and Energy Centre, United Arab Emirates University, UAE for financial support. This work was funded by the Researchers Supporting Project Number (RSPD2025R667), King Saud University, Riyadh, Saudi Arabia.

References

[1] M. Mladenov, R. Stoyanova, E. Zhecheva, S. Vassilev, Structural characterization of Mg treated $LiCoO_2$ intercalation compounds, Electrochem. Commun. 3 (2001) 410, https://doi.org/10.1007/978-94-010-0389-6_31.

[2] V. Aravindan, J. Gnanaraj, Y.-S. Lee, S. Madhavi, Insertion–type electrodes for nonaqueous Li – ion capacitors, Chem. Rev. 114 (2014) 11619–11635, https://doi.org/10.1021/cr5000915.

[3] Zheng ping Zhou, Xiang-Fa Wu, Graphene-beaded carbon nanofibers for use in supercapacitor electrodes: synthesis and electrochemical characterization, J. Power Sources 222 (2013) 410–416, https://doi.org/10.1016/j.jpowsour.2012.09.004.

[4] V.V.N. Obreja, On the performance of supercapacitors with electrodes based on carbon nanotubes and carbon activated material, Phys. E: Low Dimension.Syst. Nanostruct. 40 (2008) 2596–2605, https://doi.org/10.1016/j.physe.2007.09.044.

[5] G. Godillot, P.-L. Taberna, B. Daffos, P. Simon, C. Delmas, L. Guerlou-Demourgues, High power density aqueous hybrid supercapacitor combining activated carbon and highly conductive spinel cobalt oxide, J. Power Sources 331 (2016) 277–284, https://doi.org/10.1016/j.jpowsour.2016.09.035.

[6] Byung-Gwan Lee, Seung-Hwan Lee, Hyo-Jin Ahn, Jung-Rag Yoon, High performance hybrid supercapacitors using granule Li4Ti5O12/Carbon nanotube anode, J. Alloys Compd. 748 (2018) 882–888, https://doi.org/10.1016/j.jallcom.2018.03.248.

[7] J.Richards Joshua, V. Sharmila, A. Viji, Electrochemical performance of spongy snowballs of O_3-$NaFeO_2$@SnO: cathodes for sodium ion batteries, Int. J. Energy Res. 2023 (2023) 6616567, https://doi.org/10.1155/2023/6616567.

[8] J. Richards Joshua, Y.S. Lee, T. Maiyalagan, N. Nallamuthu, P. Yuvraj, N. Sivakumar, $Na_{0.4}(Mn_{0.33}Co_{0.33}Ni_{0.33})O_2$ surface grafted with SnO nanorods: a cathode material for rechargeable sodium ion batteries, J. Electroanal. Chem. 856 (2020) 113633, https://doi.org/10.1016/j.jelechem.2019.113633.

[9] J.B. Wu, J.P. Tu, Z. Yu, X.B. Zhang, Electrochemical investigation of carbon nanotubes as additives in positive electrodes of Ni / MH batteries, J. Electrochem. Soc. 153 (2006) A1847, https://doi.org/10.1149/1.2234592.

[10] J.Y. Xiang, J.P. Tu, J. Zhang, J. Zhong, D. Zhang, J.P. Cheng, Incorporation of MWCNTs into leaf-like CuO nanoplates for superior reversible Li-ion storage, Electrochem. Commun. 12 (2010) 1103–1107, https://doi.org/10.1016/j.elecom.2010.05.039.

[11] Xinlu Li, Feiyu Kang, Xinde Bai, Wanci Shen, A novel network composite cathode of $LiFePO_4$/multiwalled carbon nanotubes with high rate capability for lithium ion batteries, Electrochem. Commun. 9 (2007) 663–666, https://doi.org/10.1016/j.elecom.2006.10.050.

[12] Bo Jin, En Mei Jin, Kyung-Hee Park, Hal-Bon Gu, Electrochemical properties of $LiFePO_4$-multiwalled carbon nanotubes composite cathode materials for lithium polymer battery, Electrochem. Commun. 10 (2008) 1537–1540, https://doi.org/10.1016/j.elecom.2008.08.001.

[13] Fen Li, Xue Jiang, Jijun Zhao, Shengbai Zhang, Graphene oxide: a promising nanomaterial for energy and environmental applications, Nano Energy 16 (2015) 488–515, https://doi.org/10.1016/j.nanoen.2015.07.014.

[14] Zhen Cui, Hanxiao Wang, Yi Luo, Enling Li, Yang Shen, Ke Qin, Yuan Pei, Mxenes/WSSe heterojunction photodetector with ultrahigh sensitivity and accuracy, Appl. Surf. Sci. 684 (2025) 161853, https://doi.org/10.1016/j.apsusc.2024.161853.

[15] Shreyas Tiwari, Rajesh Saha, Tarun Varma, Impact of hindrance and trap impurities on the sensitivity measurement of N-Pocket TFET-based biosensor, Micro Nanostruct. 198 (2025) 208067, https://doi.org/10.1016/j.micrna.2024.208067.

[16] Xin Gao, Zhen Cui, Pengfei Wu, A two-dimensional AlN/Zr_2CO_2 heterojunction with favorable photocurrent and carrier mobility, J. Alloys Compd. 1017 (2025) 179127, https://doi.org/10.1016/j.jallcom.2025.179127.

[17] Zhen Cui, Haotian Meng, Chunli Zhang, Lin Zhang, Shuang Zhang, Lu Wang, MoSSe/Si9C15 heterojunction photodetectors with ultrahigh photocurrent and carrier mobility, Mater. Sci. Semicond. Process. 182 (2024) 108705, https://doi.org/10.1016/j.mssp.2024.108705.

[18] Zhen Cui, Hanxiao Wang, Yang Shen, Ke Qin, Pei Yuan, Enling Li, The excellent electrocatalytic HER activity and photogalvanic effect of WS_2/Ga_2O_3 based on density functional theory, Int. J. Hydrogen Energy 88 (2024) 898–905, https://doi.org/10.1016/j.ijhydene.2024.09.278.

[19] Zhen Cui, Nan Liu, Yize Zhang, Mingjun Wang, Tunable dual-broadband terahertz absorber based on vanadium dioxide stacked with multilayer structures, Opt. Commun. 570 (2024) 130874, https://doi.org/10.1016/j.optcom.2024.130874.

[20] Divya Yadav, Rajni Bala, Sumit Chauhan, Sanjay Gaur, Structural and optical investigations of lithium-modified lead bismuth borate glasses, Solid State Commun. 399 (2025) 115859, https://doi.org/10.1016/j.ssc.2025.115859.

[21] Guoqing Zhang, Zhen Cui, Aming Song, Shuang Zhang, Lu Wang, Self-powered photodetector of GaN/Sc_2CCl_2 heterojunction with high carrier mobility and polarization sensitivity, Phys. Chem. Chem. Phys. 27 (2025) 6875–6886, https://doi.org/10.1039/D4CP04162C.

[22] W. Yuan, J. Yan, Z. Tang, O. Sha, J. Wang, W. Mao, L. Ma, Preparation and electrochemical performance of Na-doped $Li_3V_2(PO_4)_3$/C cathode material, J. Power Sources 201 (2012) 301–306, https://doi.org/10.1007/s10008-012-1764-x.

[23] J.B. Goodenough, Y. Kim, Challenges for rechargeable Li batteries, Chem. Mater. 22 (2009) 587–603, https://doi.org/10.1021/cm901452z.

[24] A.S. Hameed, M.V. Reddy, B.V.R. Chowdari, J.J. Vittal, Phosphate-based cathodes and reduced graphene oxide composite anodes for energy storage applications, Electrochim. Acta 128 (2014) 184–191, https://doi.org/10.1007/978-981-10-2302-6.

[25] R. Satish, V. Aravindan, W.C. Ling, J.B. Goodenough, S. Madhavi, Carbon–coated $Li_3Nd_3W_2O_{12}$: a high power and low- voltage insertion anode with exceptional cycleability for Li–Ion batteries, Adv. Energy Mater. 4 (2014) 1301713, https://doi.org/10.1002/aenm.201301715.

[26] Xiuli Su, Jingyuan Liu, Congcong Zhang, Tao Huang, Yonggang Wang, Aishui Yu, High power lithium-ion battery based on a $LiMn_2O_4$ nanorod cathode and a carbon-coated $Li_4Ti_5O_{12}$ nanowire anode, Phys. Chem. 14 (2012) 5808–5814, https://doi.org/10.1039/C6RA23590E.

[27] S.-C. Yin, H. Grondey, P. Strobel, M. Anne, L.F. Nazar, Electrochemical property: structure relationships in Monoclini $Li_{3-y}V_2(PO_4)_3$, J. Phys. Chem. C 112 (2008) 5689–5693, https://doi.org/10.1021/ja034565h.
[28] J. Jayachitra, J. Richards Joshua, A. Balamurugan, N. Sivakumar, V. Sharmila, S. Shanavas, Mohammad Abu Haija, Mir Waqas Alam, Amal BaQais, High electrode performance of hydrothermally developed activated C coated O3–$NaFeO_2$ electrode for Na-ion batteries applications, Ceram. Int. 49 (2023) 48–56, https://doi.org/10.1016/j.ceramint.2022.07.110.
[29] S.-C. Yin, P.S. Strobel, H. Grondey, L.F. Nazar, $Li_{2.5}V_2(PO_4)_3$: a Room- temperature analogue to the fast–ion conducting high–temperature γ-Phase of $Li_3V_2(PO_4)_3$, J. Chem mater. B 110 (2006) 171–177, https://doi.org/10.1021/cm034802f.
[30] N. Kalaiselvi, C.-H. Doh, C.-W. Park, S.-I. Moon, M.-S. Yun, A novel approach to exploit $LiFePO_4$ compound as an ambient temperature high-capacity anode material for rechargeable lithium batteries, Electrochem. Commun. 6 (2004) 1110, https://doi.org/10.1016/j.elecom.2004.08.014.
[31] Fu Peng, Yanming Zhao, Youzhong Dong, Xiaoning An, Guopei Shen, Synthesis of $Li_3V_2(PO_4)_3$ with high performance by optimized solid-state synthesis routine, J. Power Sources 162 (2006) 651–657, https://doi.org/10.1016/j.jpowsour.2006.07.029.
[32] X.J. Zhu, Y.X. Liu, L.M. Geng, L.B. Chen, Synthesis and performance of lithium vanadium phosphate as cathode materials for lithium ion batteries by a sol–gel method, J. Power Sources 184 (2008) 578–582, https://doi.org/10.1016/j.jpowsour.2008.01.007.
[33] Ping Hu, Mengyu Yan, Ting Zhu, Xuanpeng Wang, Xiujuan Wei, Jiantao Li, Zhou, Zn/V_2O_5 aqueous hybrid – ion battery with high voltage platform and long cycle life, ACS Appl. Mater. Interfaces 9 (2017) 1437–1445, https://doi.org/10.1021/acsami.7b13110.
[34] Yongjin Fang, Xin-Yao Yu, X.W.D. Lou, Nanostructured electrode materials for advanced sodium-ion batteries, Matter 10 (2017) 1757–1763, https://doi.org/10.1016/j.matt.2019.05.007.
[35] Wangjia Tang, Jianbo Wu, Xiuli Wang, Xinhui Xia, Jiangping Tu, Integrated carbon nanospheres arrays as anode materials for boosted sodium ion storage, Green Energy Environ. 3 (2018) 50–55, https://doi.org/10.1016/j.gee.2017.08.001.
[36] H. Huang, S.C. Yin, T. Kerr, N. Taylor, L.F.A. Nazar, High capacity, fast rate $Li_3V_2(PO_4)_3$/Carbon cathode for rechargeable lithium batteries, Adv. Mater. 14 (2002) 1525, https://doi.org/10.1002/1521-4095(20021104.
[37] S.C. Yin, H. Grondey, P. Strobel, M. Anne, L.F. Nazar, $Li_{2.5}V_2(PO_4)_3$: a room-temperature analogue to the fast-ion conducting high-temperature γ-Phase of $Li_3V_2(PO_4)_3$, J. Am. Chem. Soc. 125 (2003) 10402, https://doi.org/10.1021/cm034802f.
[38] J. Richards Joshua, T. Maiyalagan, N. Sivakumar, Y.S. Lee, Advanced High Voltage Cathode Materials for Rechargeable Lithium Ion Batteries, 1, CRC Press, 2020, p. 33, https://doi.org/10.1201/9781351052702.
[39] Zhizhen Zhang, Pierre-Nicholas Roy, Hui Li, Maxim Avdeev, Linda F. Nazar, Coupled cation–anion dynamics enhances cation mobility in Room- temperature superionic solid-state electrolytes, J. Am. Chem. Soc. 125 (2003) 10402–10411, https://doi.org/10.1021/jacs.9b09343.
[40] Z. Li, Z. Zhou, X.P. Gao, J. Yan, Electrochemical performance of $LiVPO_4F$/C synthesized by different methods, J. Power Sources 160 (2006) 633, https://doi.org/10.1016/S1003-6326(12)61702-6.
[41] J. Jayachitra, J. Richards Joshua, A. Balamurugan, N. Sivakumar, V. Sharmila, High electrode performance of hydrothermally developed activated C coated O3–$NaFeO_2$ electrode for Na-ion batteries applications, Ceram. Int. 49 (2023) 48–56, https://doi.org/10.1016/j.ceramint.2022.07.110.
[42] Xiaoke Zhi, Guangchuan Liang, Li Wang, Xiuqin Ou, Limin Gao, Xiaofei Jie, Optimization of carbon coatings on $LiFePO_4$: carbonization temperature and carbon content, J. Alloys Compd. 503 (2010) 370–374, https://doi.org/10.1016/j.jallcom.2010.02.173.
[43] Tao Jiang, Chunzhong Wang, Gang Chen, Hong Chen, Yingjin Wei, Xu Li, Effects of synthetic route on the structural, physical and electrochemical properties of $Li_3V_2(PO_4)_3$ cathode materials, Solid State Ionics 180 (2009) 708–714, https://doi.org/10.1016/j.ssi.2009.02.027.
[44] Tao Jiang, Fei Du, Kejin Zhang, Yingjin Wei, Zhe Li, Chunzhong Wang, Gang Chen, Effects of carbon coating on the temperature-dependent electrochemical properties of $Li_3V_2(PO_4)_3$, Solid State Sci. 12 (2010) 1672–1676, https://doi.org/10.1016/j.solidstatesciences.2010.07.023.
[45] Tao Jiang, Wencheng Pan, Jian Wang, Xiaofei Bie, Fei Du, Yingjin Wei, Chunzhong Wang, Gang Chen, Carbon coated $Li_3V_2(PO_4)_3$ cathode material prepared by a PVA assisted sol–gel method, Electrochim. Acta 55 (2010) 3864–3869, https://doi.org/10.1016/j.electacta.2010.02.026.
[46] X.H. Rui, N. Ding, J. Liu, Analysis of the chemical diffusion coefficient of lithium ions in $Li_3V_2(PO_4)_3$ cathode material, Electrochim. Acta 55 (2010) 2384–2390, https://doi.org/10.1016/j.electacta.2009.11.096.
[47] Bo Jin, En Mei Jin, Kyung-Hee Park, Hal-Bon Gu, Electrochemical properties of $LiFePO_4$-multiwalled carbon nanotubes composite cathode materials for lithium polymer battery, Electrochem. Commun. 10 (2008) 37–1540, https://doi.org/10.1016/j.elecom.2008.08.001.
[48] Amit Mishra, Akansha Mehta, Nagaraj P. Shetti, Electrode materials for lithium-ion batteries, J. Mater. Sci. Energy Tech. 1 (2007) 182–187, https://doi.org/10.1016/j.mset.2018.08.001.
[49] Liu Jie-qun, Sheng-kui Zhong, Ling Wu, Wan Kang, Lu Fan, Electrochemical performance of $LiVPO_4F$/C synthesized by different methods, Trans. Nonferrous Metals Soc. China 229 (2012) 156, https://doi.org/10.1016/S1003-6326(12)61702-6.
[50] Jie-xi wang, Zhi-xing, Li Shen, Xin hai Al, Hua-jun Guo, Synthesis and performance of $LiVPO_4F$/C based cathode materials for lithium-ion battery, Trans. Nonferrous Metals Soc. China 239 (2013) 1718–1722, https://doi.org/10.1016/S1003-6326(13)62653-9.
[51] Shengkui Zhong, Wei Hong, Xiaoping Zhang, Jiequm Liu, Yunxiang Li, Yanling Shi Ling Wu, Synthesis of $xLiVPO_4F.yLi3V_2(PO_4)_3$/C composite as potential cathode material for Li-ion batteries, Ionics 23 (2017) 803–819, https://doi.org/10.1007/s11581-016-1875-y.
[52] Zelang Jian, Wenze Han, Yanliang Liang, Yucheng Lan, Zheng Fang, Yong-Sheng Hud, Yan Yao, Carbon-coated Rhombohedral $Li_3V_2(PO_4)_3$ as both anode and cathode materials for lithium-ion batteries: electrochemical performance and lithium storage mechanism, J. Mater. Chem. A 2 (2014) 20231, https://doi.org/10.1039/C4TA04630G.
[53] Xianhong Rui, Qingyu Yan, Maria Skyllas-Kazacos, Tuti Mariana Lim, $Li_3V_2(PO_4)_3$ cathode materials for lithium-ion batteries: a review, J. Power Sources 258 (2014) 19–38, https://doi.org/10.1016/j.jpowsour.2014.01.126.